DETERMINING THE SEVERITY OF OBSTRUCTIVE SLEEP APNEA (OSA) BY USING NUMERICAL ANALYSIS

ANG MING LOK

**FACULTY OF ENGINEERING
UNIVERSITY OF MALAYA
KUALA LUMPUR**

2020

DETERMINING THE SEVERITY OF OBSTRUCTIVE SLEEP APNEA (OSA) BY USING NUMERICAL ANALYSIS

ANG MING LOK

RESEARCH PROJECT SUBMITTED IN PARTIAL FULFILMENT OF THE REQUIREMENTS FOR THE DEGREE OF MASTER OF MECHANICAL ENGINEERING

2020

UNIVERSITY OF MALAYA

ORIGINAL LITERARY WORK DECLARATION

Name of Candidate: Ang Ming Lok

Matric No: 17201702 OR KQK190012

Name of Degree: Master of Mechanical Engineering

Title of Research Project ("this Work"):

Determining the Severity of Obstructive Sleep Apnea (OSA) by using Numerical Analysis

Field of Study: Numerical Analysis

I do solemnly and sincerely declare that:

(1) I am the sole author/writer of this Work;
(2) This Work is original;
(3) Any use of any work in which copyright exists was done by way of fair dealing and for permitted purposes and any excerpt or extract from, or reference to or reproduction of any copyright work has been disclosed expressly and sufficiently and the title of the Work and its authorship have been acknowledged in this Work;
(4) I do not have any actual knowledge nor do I ought reasonably to know that the making of this work constitutes an infringement of any copyright work;
(5) I hereby assign all and every rights in the copyright to this Work to the University of Malaya ("UM"), who henceforth shall be owner of the copyright in this Work and that any reproduction or use in any form or by any means whatsoever is prohibited without the written consent of UM having been first had and obtained;
(6) I am fully aware that if in the course of making this Work I have infringed any copyright whether intentionally or otherwise, I may be subject to legal action or any other action as may be determined by UM.

Candidate's Signature Date:

Subscribed and solemnly declared before,

Witness's Signature Date:

Name:

Designation:

DETERMINING THE SEVERITY OF OBSTRUCTIVE SLEEP APNEA (OSA) BY USING NUMERICAL ANALYSIS

ABSTRACT

Computational technologies and biomechanical theories have been applied to study upper airway mechanics in obstructive sleep apnea (OSA). In this study, the patient is selected from ENT Department, UMMC, diagnosed with mild to severe OSA. In addition, the patient underwent maxillomandibular advancement (MMA) surgical treatment. Therefore, 3-dimensional modeling software will be used to model the upper airway, based on patient specific geometrical characteristics obtained from medical imaging and computed tomography (CT). Hence, providing an accurate assessment of airflow characteristics. Computational fluid dynamics (CFD) analysis will be combined with upper airway geometries obtained before and after surgical to determine the effects on parameters, such as, pressure drop and turbulent kinetic energy. Moreover, Patient-specific airway geometries obtained from CT scans is used to determine treatment therapy for OSA syndrome. CFD is therefore an attractive method to model treatment outcome in OSA patient-specific airway geometry before implementation of treatment devices or performing surgery.

Keywords: Computational Fluid Dynamics (CFD), Obstructive Sleep Apnea (OSA), Human Upper Airway (HUA), Maxillomandibular Advancement (MMA), Turbulence.

ACKNOWLEDGEMENTS

I would like to thank Prof Madya Ir. Dr. Nik Nazri bin Nik Ghazali for his guidance on this research project and for providing this platform to deepen my understanding in computational fluid dynamics.

I would like to thank my parents and sister for their constant support and encouragement during my whole master education.

TABLE OF CONTENTS

Abstract iii

Acknowledgements iv

Table of Contents v

List of Figures vii

List of Tables.. ix

List of Symbols and Abbreviations... x

CHAPTER 1: INTRODUCTION 1

1.1 Background 1

1.1.1 Human Respiratory Tract Anatomy 1

1.1.2 Obstructive Sleep Apnea 3

1.1.3 Treatment for Obstructive Sleep Apnea 4

1.2 Objectives and Scope of Study 5

1.2.1 Motivation 5

1.2.2 Objectives 5

1.2.3 Scope of Study 6

CHAPTER 2: LITERATURE REVIEW 7

2.1 Human Upper Airway Airflow Analysis 7

2.1.1 Human Respiration 7

2.1.2 Effect of Obstructive Sleep Apnea on the Airway 8

2.2 Computational Fluid Dynamics Approaches 10

2.2.1 Pharyngeal Airway Modeling 11

2.2.2 Computation Methods 13

CHAPTER 3: METHODOLOGY **15**

3.1 Three-Dimensional Modelling of the Human Upper Airway 15

3.2 Mesh Generation 18

3.3 Computational Fluid Dynamics Simulation 20

3.3.1 Governing Equations 20

3.3.2 Numerical Methods 21

3.3.3 Mesh Independence Test 22

CHAPTER 4: RESULTS AND DISCUSSION **23**

4.1 Morphology Effect of Maxillomandibular Advancement 23

4.2 Computational Fluid Dynamics Turbulence Modeling 23

4.3 Turbulent Flow in the Domain 26

4.4 Collapsibility of the Soft Tissue 27

4.5 Computational Fluid Dynamics Study on Maxillomandibular Advancement 27

CHAPTER 5: CONCLUSION AND RECOMMENDATIONS **29**

5.1 Conclusion 29

5.2 Recommendations for Future Work 29

References 30

LIST OF FIGURES

Figure 1.1: Diagram of the human respiratory system.. 2

Figure 1.2: Diagram of the human upper airway. 2

Figure 2.1: Variation of in the upper airway area at the retroglossal level during respiration of the same subject. (Schwab et al., 1993).. 9

Figure 2.2: Lateral view of a segmented model of the nasal cavity and pharynx. (Jeong et al., 2007).. 10

Figure 2.3: Single slice of the CT scan rendered on greyscale, with linear scale (top) and with emphasis on the air (bottom). (Quadrio et al., 2016) 12

Figure 2.4: Meshing of the reconstructed pharyngeal airway. (Fan et al., 2020) 13

Figure 3.1: Pre-OP CT scan of the patient viewed using Mimics. Axial, coronal, sagittal and 3D views (counterclockwise starting from top right)... 15

Figure 3.2: Post-OP CT scan of the patient viewed using Mimics. Axial, coronal, sagittal and 3D views (counterclockwise starting from top right)... 16

Figure 3.3: Thresholding of pre-OP CT scan to generate mask.................................... 16

Figure 3.4: Thresholding of post-OP CT scan to generate mask. 17

Figure 3.5: Pre-OP 3D model of the velopharynx region in the respiratory tract (yellow region). 17

Figure 3.6: Post-OP 3D model of the velopharynx region in the respiratory tract (yellow region). 18

Figure 3.7: Surface elements of the pre-op model. 19

Figure 3.8: Enlarged view of the internal volume element of the pre-op model. 19

Figure 3.9: Surface elements of the post-op model. 20

Figure 3.10: Enlarged view of the internal volume element of the post-op model......... 20

Figure 4.1: Wall surface pressure contour of (a) pre-op and (b) post-op velopharynx models. 24

Figure 4.2: Velocity contour of (a) pre-op and (b) post-op velopharynx mid-sagittal plane. 25

Figure 4.3: Turbulence kinetic energy contour of (a) pre-op and (b) post-op velopharynx mid-sagittal plane. 26

Figure 4.4: Wall shear stress contour of (a) pre-op and (b) post-op velopharynx models. 26

LIST OF TABLES

Table 3.1: Number of 3D tetrahedral elements in each corresponding mesh. 22

Table 4.1: Comparison between pre- and post-op airway geometry. 23

Table 4.2: Airflow properties of turbulence modeling. 24

Table 4.3: Airflow properties at the inlet and outlet region on the anterior wall of the velopharynx. 25

LIST OF SYMBOLS AND ABBREVIATIONS

HUA	:	Human upper airway
OSA	:	Obstructive sleep apnea
2D	:	Two-dimensional
3D	:	Three-dimensional
CT	:	Computer tomography
AHI	:	Apnea-hypopnea index
RDI	:	Respiratory distress index
CPAP	:	Continuous positive airway pressure
MMA	:	Maxillomandibular advancement
SDB	:	Sleep disordered breathing
MRI	:	Magnetic resonance imaging
RANS	:	Reynolds-averaged Navier-Stokes
LES	:	Large eddy simulation
DNS	:	Direct numerical simulation
SGS	:	Sub-grid scale
HU	:	Hounsfield unit
Re	:	Reynolds number

CHAPTER 1: INTRODUCTION

1.1 Background

The human respiratory system performs the vital process of breathing, which supplies one of basic requirements of life. The respiratory system comprises the upper and the lower airway system. The lungs, located at the lower airway system, play an important role in the breathing process, as gas exchange takes place in the blood stream of this organ. Oxygen is supplied into the blood stream, while carbon dioxide is removed. The upper airway serves as a connection between the atmosphere and the lower segment of the respiratory system, providing the lungs filtered and treated air. Therefore, any obstruction of the upper airway has the severity of a malfunctioning lungs.

Within the past decades, dysfunction of human upper airway (HUA) has become the dominant pathology for obstructive sleep apnea (OSA) syndrome studies. The medical and dental communities were mainly focused on treatment for OSA and neglected the dynamics of the syndrome. Initial investigations of the three-dimensional airway are limited to two-dimensional (2D) analysis (i.e. radiography) (Tawhai et al., 2004).

In the recent years, with increased computational capabilities, researchers started to utilize three-dimensional (3D) numerical simulations to analyze the causation of OSA. 3D models are generated using computed tomography (CT) scans of the human airway (Kim et al., 2018; Lopez et al., 2019). However, accurate modeling of the HUA passage is required to represent the subject of study.

1.1.1 Human Respiratory Tract Anatomy

The human respiratory airway begins with the external nose and ends at the lungs as shown in Figure 1.1. The upper respiratory tract consists of the nasal cavity and the throat (pharynx). Along the superior of the nasal cavity are the olfactory receptors, which enable human beings the sense of smell.

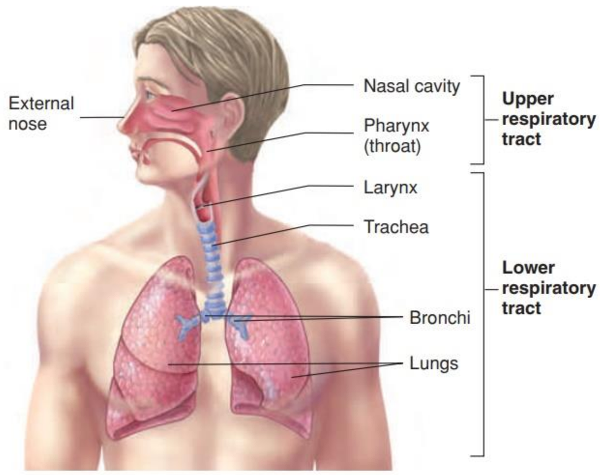

Figure 1.1: Diagram of the human respiratory system

The pharynx consists of three segments: the hypopharynx, the oropharynx, and the nasopharynx, as shown in Figure 1.2. Moreover, the nasopharynx connects the nasal and oral cavity, which allows human beings to breathe through the nose and the mouth. Situated at the posterior of the oral cavity, the oropharynx serves as a passageway for food to enter the esophagus and for air to flow to and from the windpipe (trachea). The hypopharynx is the junction where the digestive passage and respiratory passage converges. As both food and air pass through the pharynx, a connective tissue called the epiglottis closes over the trachea when food is swallowed to inhibit aspiration.

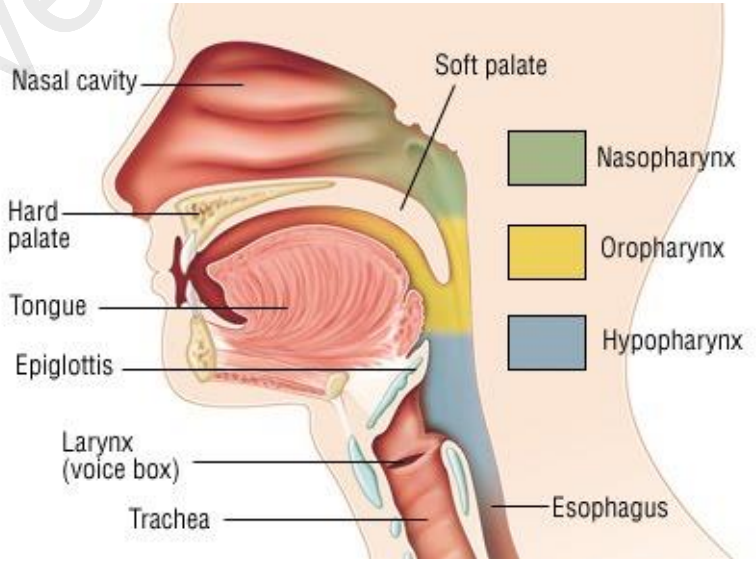

Figure 1.2: Diagram of the human upper airway.

1.1.2 Obstructive Sleep Apnea

Obstructive sleep apnea (OSA) is a chronic disease characterized as repetitive partial or complete collapse of the upper airway resulting in complete stoppage (apnea) or reduced airflow (hypopnea) (Eckert & Malhotra, 2008). The typical symptoms of OSA are breathing interruption, loud snoring, awakening from sleep, and excessive daytime sleepiness (Johns, 1993), but other symptoms such as morning headaches, irritability, memory problems, and fatigue are also common (Partinen, 1995).

The common cause of OSA is the relaxation of soft tissues in the upper airway, particularly in the oropharynx region (Wilhelm et al., 2015), and gravity promotes the fall back of the soft tissues and tongue to the throat area. Another factor that encourages OSA is the sleeping position, as the supine position demonstrates increased favorability in collapsibility of the soft tissue (Joosten et al., 2014). Other factor that predispose the occurrence of OSA includes increased thickness of the pharyngeal wall due to obesity (Pinto et al., 2011).

Severity of OSA is classified by indexes such as the apnea-hypopnea index (AHI) or respiratory distress index (RDI) by means of standard sleep-related questions and nocturnal polysomnography (Hoffstein & Szalai, 1993). The AHI index is a measure of average number of apneas and hypopneas occurrence in an hour of sleep. The American Academy of Sleep Medicine (AASM) categorizes the index under three classifications: mild OSA (5-15 occurrences/hour), moderate OSA (15-30 occurrences/hour), and severe OSA (more than 30 occurrences/hour). The RDI index includes more subtle respiratory irregularities, such as respiratory-effort related arousals (RERAs). RERAs are breathing disorders that lead to sleep arousal but does not meet the criteria of apnea or hypopnea (Cirignotta, 2004).

1.1.3 Treatment for Obstructive Sleep Apnea

Currently, there are several treatment options for obstructive sleep apnea of varying intrusiveness. Non-surgical treatments such as weight loss, continuous positive airway pressure (CPAP), oral appliances, positional therapy, and medication, (Lam et al., 2007; Oksenberg et al., 2006; Schmidt-Nowara et al., 1995; Strobel & Rosen, 1996) are the first-line of approaches to OSA. Surgical treatments are recommended as the secondary option if non-surgical method fails. These treatments for OSA includes nasal surgery, upper airway surgery, maxillomandibular advancement (MMA), tracheostomy, and hypoglossal nerve stimulation (Hochban et al., 1994; Kezirian et al., 2014; Nakata et al., 2005; Sher, 2002; Thatcher & Maisel, 2003).

Obesity is clinically defined as an individual with at least 120% of their ideal body weight. The ideal body weight is assessed based on the numerical statistics of the weight associated with the morbidity rate of a specific height. Two thirds of 1000 OSA patients are classified as obese with at least 130% of their ideal weight (Williams et al., 1988). Multiple studies have shown a varied amount of weight loss has proven an improvement in sleep disordered breathing (SDB) and sleep quality (Strobel & Rosen, 1996).

For mild to moderate severity of OSA, non-surgical treatment such as CPAP is widely recommended as the treatment of choice (TL Giles et al., 2006). Conservative measures and oral appliance are alternative approaches to CPAP in treating mild to moderate OSA. However, CPAP is proven to be the superior methodology in improving daytime sleepiness, SDB parameters, and sleepiness factor (Lam et al., 2007). For severe cases of OSA, non-surgical treatments are performed initially before attempting the surgical measures (Guilleminault & Stoohs, 1990). Surgical alteration such as MMA moves the upper and lower jaws forward to enlarge the airway. OSA syndrome is alleviated as indicated from postoperative RDI of less than 10 (Hochban et al., 1994).

1.2 Objectives and Scope of Study

1.2.1 Motivation

As discussed previously, obstructive sleep apnea has the severity of malfunction lungs and nearly 80% of men and 93% of women with moderate to severe sleep apnea are undiagnosed in the community. Moreover, in Malaysia, treatment through the oral appliances is uncommon and there is no structured flow from the engineering to the medical in the classification of OSA. Thus, there is a great need for further research in this field. In addition, there are no other research that involve numerical investigation of the airway and oral soft tissue changes among Malaysians.

1.2.2 Objectives

The objectives of this project are:

- To analyze computed tomography data of patient with obstructive sleep apnea by using Materialise software.
- To simulate the airway of the patient by using Ansys Fluent software to evaluate the pressure and turbulent kinetic energy.
- To classify and match the numerical analysis results with conventional apnea-hypopnea index.

1.2.3 Scope of Study

The pharyngeal airflow is assumed as steady and incompressible fluid flow. In addition, the airflow is assumed as laminar flow for flow rate below 0.2 L/s and turbulent flow for flow rate above 0.2 L/s. Hence, the airway is simulated using flow rate of 0.5 L/s. The air density and dynamic viscosity is 1.225 kg/m ^{3} and 1.789×10^{-5} kg/m·s, respectively and assumed to be constant at 15 ℃. Moreover, the turbulent flow is modeled using k-ω turbulent model. Furthermore, the breathing process is assumed to be inspiration and nasal breathing only. Lastly, the domain of interest is located at the velopharynx as it is identified as the most collapsible region of the pharyngeal airway.

CHAPTER 2: LITERATURE REVIEW

The human upper airway is intricate and manipulated by a variety of factors. For instance, respiration itself is split into two phases, breathing in oxygen (inhalation) and breathing out carbon dioxide (exhalation). In addition, there are several types of breathing practiced by human being, such as eupnea, diaphragmatic breathing, costal breathing, and hyperpnea. Moreover, respiration can be performed through nose (nasal breathing), or mouth (oral breathing), or both together (oronasal breathing).

The physical geometry of the airway varies among each human being. Therefore, individual models must be established to conduct realistic experimentation of the subject. The geometrical model can be reconstruction from 3D computed tomography images of the patient upper airway (Lopez et al., 2019). Besides that, implementation of computational fluid dynamics has enabled identification of the severity markers of OSA through flow simulations (Vos et al., 2007).

2.1 Human Upper Airway Airflow Analysis

2.1.1 Human Respiration

Human beings respire cyclically at frequency between 6 and 31 breaths per minute, and tidal volume (lung volume) in the range of 442 and 1549 ml (Benchetrit, 2000). In addition, the ventilation minute volume (volume of gas inhaled per minute) in four main activities are estimated: 0.125 L/s during sleep, 0.15 L/s during sitting, 0.42 L/s during light physical activity, and 0.83 L/s during heavy physical activity (Roy et al., 1994). The peak nasal inspiratory flow (PNIF) is rated at 2.38 L/s for male and 2.03 L/s for female (Ottaviano et al., 2006). However, study shows a healthy human being will change from nasal breathing to oronasal breathing at flow rate of 0.58 L/s before achieving PNIF rate (Niinimaa et al., 1980). Hence, ventilation minute volume should be capped at 0.58 L/s to simulate nasal respiration.

Fluid flow is categorized into two regimes which is governed by the Reynolds number. Laminar flow generally is experienced during low flow rate or in viscous fluid. As the flow rate increases, the fluid will transition from laminar to turbulent flow and fully developed turbulent flow is achieved when the Reynolds number threshold is exceeded. Nasal airflow is determined to be in the laminar flow regime for normal breathing through an enlarge experimental model of the HUA (Hahn et al., 1993). Furthermore, numerical study of the same HUA model verifies the laminar regime during normal breathing with flow rate below 0.2 L/s (Keyhani et al., 1995).

Transition to turbulent flow begins when flow rate exceeds 0.2 L/s and fully developed turbulent flow is attained at flow rate of 0.5 L/s (Schreck et al., 1993). Hence, respiration is further classified under three phases: laminar flow during low flow rate (less than 0.2 L/s), transitioning flow during moderate flow rate (0.2-0.5 L/s), and fully developed turbulent flow during high flow rate (more than 0.5 L/s). Moreover, breathing is typically studied by as an incompressible flow due to the Mach number of below 0.3 (Bailie et al., 2006).

2.1.2 Effect of Obstructive Sleep Apnea on the Airway

As mentioned previously, obstructive sleep apnea patients suffer repetitive partial or complete occlusion of the breathing airway. These episodes mainly occur due to yielding of the adjacent soft tissue in the pharyngeal region. Studies have shown the compliance can be related to the intensity of muscle activation, properties of respiratory airflow and pharyngeal airway tissue, and the morphology of the pharyngeal airway (S. Cheng et al., 2011; Hollandt & Mahlerwein, 2003; Huang et al., 2005; Sauerland & Harper, 1976; Schwab et al., 1995). In addition, the caliber of the airway changes throughout the respiration cycle as shown Figure 2.1. The upper airway narrows down during early inspiration then enlarges at the end of inspiration and reaches the maximum area during early expiration then narrows down (Schwab et al., 1993).

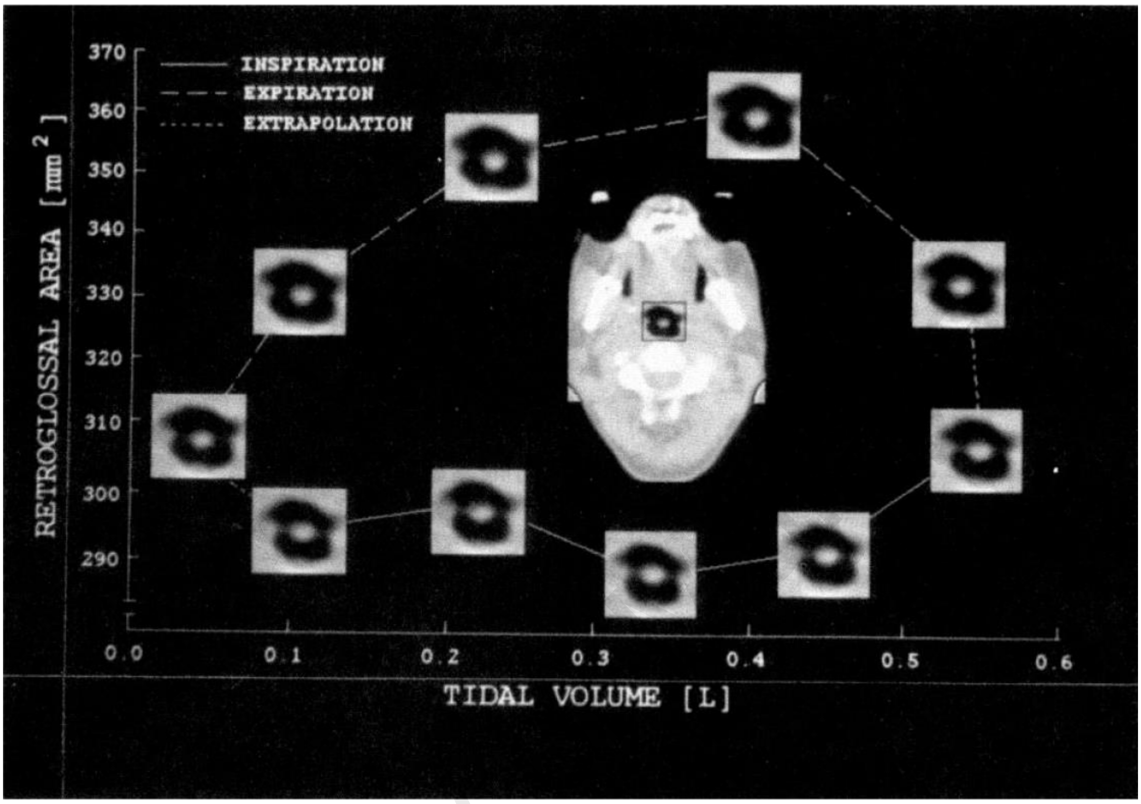

Figure 2.1: Variation of in the upper airway area at the retroglossal level during respiration of the same subject. (Schwab et al., 1993)

Despite morphology studies, numerical studies have been conducted using computational fluid dynamics to analyze the pharyngeal airway of patients with OSA (Jeong et al., 2007; Kumar et al., 2019; Lopez et al., 2019; Wang et al., 2012). The general 3D model of the airway used in CFD stimulation is shown in Figure 2.2. In addition, the model is segmented and labeled to identify the domain of interest. The following study evaluated the aerodynamic force and attributes in the HUA of a patient with OSA (in Figure 2.2). They have concluded that turbulent jet forms in the velopharynx due to passage constriction, increases the aerodynamic force acting on the region (Jeong et al., 2007). Hence, the velopharynx is considered as the most collapsible region in the pharyngeal airway.

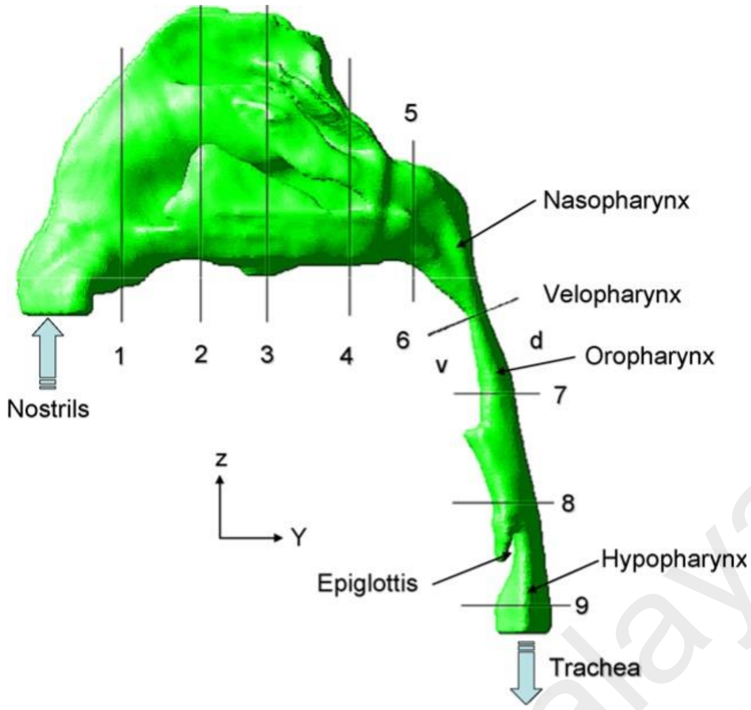

Figure 2.2: Lateral view of a segmented model of the nasal cavity and pharynx.
(Jeong et al., 2007)

2.2 Computational Fluid Dynamics Approaches

Computational fluid dynamics is widely utilized to understand the physiology and evaluate the pathology of the human respiratory airway (Leong et al., 2010). There are curtain challenges in simulating the airflow through the respiratory tract. For instance, the geometry of the airway and the characteristic of the airflow are deemed to be intricate as discussed previously. Hence, these factors are considered as the boundary conditions for the study of respiratory flow using CFD.

The application of CFD has enabled the researchers the ability to clearly visualize the result of experimentation such as the properties and patterns of the fluid flow in the HUA (Khalyfa et al., 2016). Moreover, pre-operative analysis of the several proposed surgery possibilities using CFD has established higher confidence in the clinical procedure (Mylavarapu et al., 2013). In addition, CFD is used to assess the relationship between external movement and internal airflow of the airway (Bates et al., 2019). Hence, this proves CFD is a useful tool in human airway studies.

2.2.1 Pharyngeal Airway Modeling

The modeling process is largely aided by computer software such as Ansys Workbench, Ansys TGrid, Pointwise Gridgen, AutoDesk AutoCAD, Dassault Systemes CATIA, etc. Nevertheless, the procedure typically consists of identifying the domain of interest, creating a model of the domain, and mesh generation on the domain (Faizal et al., 2020). The geometry of the pharyngeal airway is usually modeled based on the magnetic resonance imaging (MRI) or computed tomography (CT) scans. However, replicating complex structure of the human organ consumes computing memory and time. Therefore, researchers occasionally replace region outside of the domain of interest with simplified structures to reduce computational cost (Hagen et al., 2017). Conversely, researchers equipped with powerful hardware opt to model the entire airway from the nasal cavity down to the trachea (Jeong et al., 2007; Sung et al., 2006).

MRI and CT scans acquired from the radiology clinics are in forms of 2D slices in the sagittal-coronal plane as shown in the left column of Figure 2.3. On the other hand, the sagittal-axial and coronal-axial planes are reconstructed from the sagittal-coronal data set. The scans are ingested into 3D modeling software to region-grow the geometry based on the upper and lower threshold values. For airway geometry, the lower threshold value is input at typically around -1000 HU (Nakano et al., 2013). On the contrary, the upper threshold varies among the researchers. For instance, the air-filled space in the respiratory airway is segmented at threshold value around -200 to -220 HU (Lan, 2004; Quadrio et al., 2016). However, after taking into consideration of the soft tissue and mucosa lined surface of the airway, the optimum upper threshold is found to be in the range of -450 to -500 HU (Nakano et al., 2013).

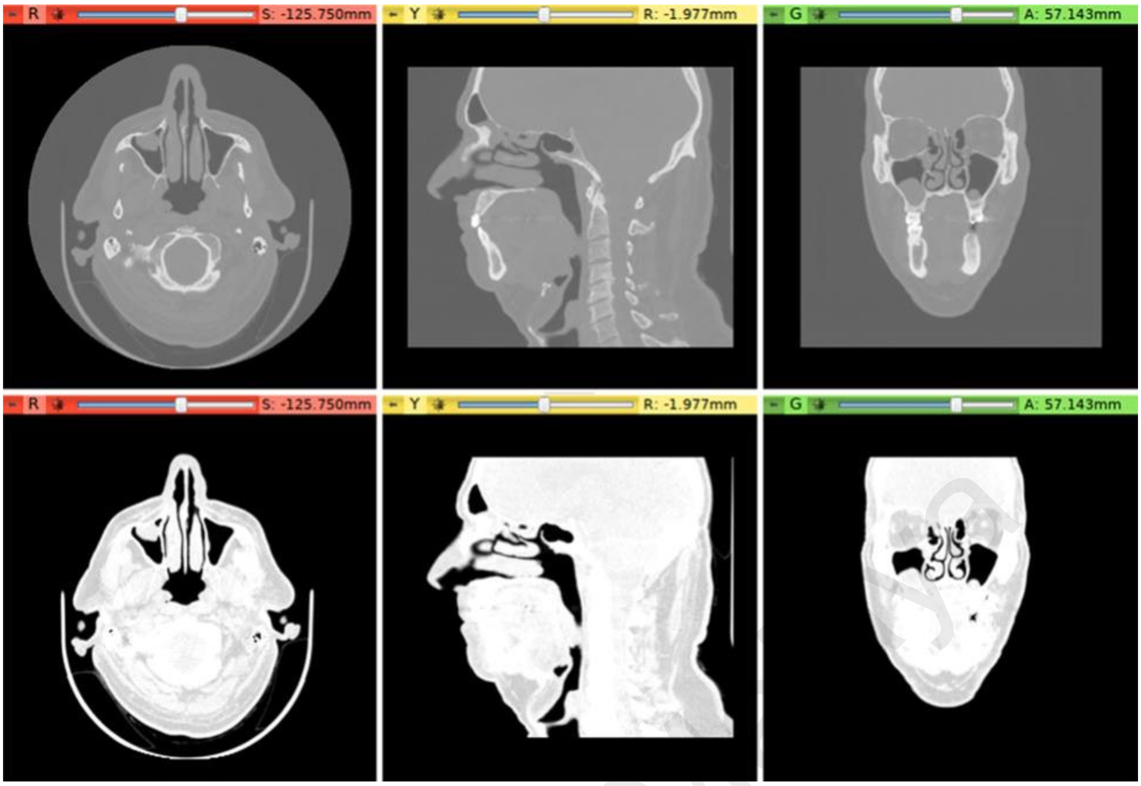

Figure 2.3: Single slice of the CT scan rendered on greyscale, with linear scale (top) and with emphasis on the air (bottom). (Quadrio et al., 2016)

The reconstructed geometry serves as an input for meshing or grid generation procedure. Surface smoothing of the geometry is necessary to reduce the skewness of the mesh (Wang et al., 2012). In addition, any uneven surface or physical discontinuity is removed to improve the surface mesh quality (Xu et al., 2006). Consequently, triangular or quadrilateral elements, and hexahedron or tetrahedron elements are generated as surface mesh and volume mesh, respectively as shown in Figure 2.4. The quality of mesh generation has equivalent importance to the boundary conditions as it affect the accuracy and stability of the CFD simulation. Moreover, the mesh independence test is carried out to identify the optimum quantity of elements or cells in the domain (Faizal et al., 2020).

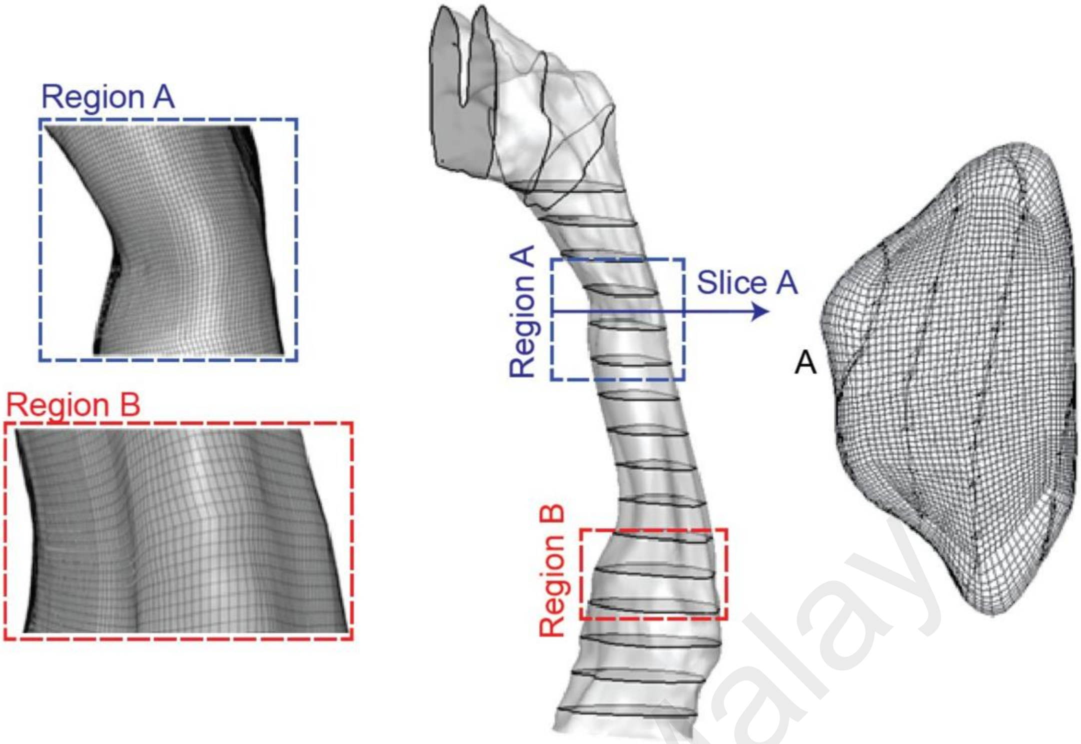

Figure 2.4: Meshing of the reconstructed pharyngeal airway. (Fan et al., 2020)

2.2.2 Computation Methods

The CFD simulation estimates the mean flow characteristics by evaluating the governing equations (i.e. Navier-Stokes equations), which consist of continuity, energy, and momentum equations. However, there are no analytical solution to the Navier-Stokes equations available currently. Hence, CFD simulation comprise of three different numerical approaches to calculate the domain: Reynolds-averaged Navier-Stokes (RANS), large eddy simulation (LES), and direct numerical simulation (DNS).

The RANS approach solves the time-averaged Navier-Stokes using two-equation turbulence models which calculates two differential-transport equations. The common transport equation among the models is symbolized as turbulent kinetic energy (k), whereas the other equation is either the dissipation rate of turbulent kinetic energy (ε) or the specific dissipation rate of turbulent kinetic energy (ω). However, RANS is unable to describe statistically unsteady flow field such as vortex structure development.

The LES approach solves the spatially averaged Navier-Stokes which includes large vortices in turbulent flow analysis. In this approach, large eddies are directly predicted, but eddies smaller than the mesh are modeled using sub-grid scale (SGS). On the other hand, the DNS approach numerically solves the unsteady Navier-Stokes equations and resolves the full spectrum of the turbulent scale. However, the downside to the LES and DNS approaches is the amount of computational resources required to calculate and predict the turbulent flow.

The selection of the solver method is a balance between computational time and resolution of the CFD result. In addition, most of the respiratory airway CFD studies simulates the steady inspiration flow instead of the entire respiration cycle, which does not involve unsteady flow field (Faizal et al., 2019). Hence, two-equation RANS models are considered as the practical solvers to simulate the human upper airway (Launder & Spalding, 1974). Moreover, the k-ω model has higher accuracy when compared to the k-ε model in a comparison study between RANS and LES approaches in a realistic pharyngeal airway model (Mihaescu et al., 2008).

CHAPTER 3: METHODOLOGY

3.1 Three-Dimensional Modelling of the Human Upper Airway

The geometry of the human upper airway is reconstructed by pre-processing the CT or MRI scans of the patient. The CT scans usually contain pixels representing its relative radiodensity in greyscale. Moreover, the pixel value ranges from -1024 to +3071 on the Hounsfield scale. Individual object attenuates at its own Hounsfield unit (HU), for instance, air has an attenuation value of -1000 HU, while water has value of 0 HU. In addition, titanium implant is at +1000 HU and hard bone can reach up to +2000 HU. Likewise, MRI images are also displayed in greyscale, in which different object correspond to different value in the black and white spectrum. Hence, the exact location and geometry of the human organ can be mapped out using CT or MRI scans.

Pre- and post-OP CT scans of the OSA patient were segmented using Mimics Research 21.0 (Materialise, Leuven, Belgium). The imported CT scans are presented in greyscale as shown in Figure 3.1 and 3.2. The axial view displays the original slice from the CT scans, while the remaining views are generated through interpolation of the pixel values.

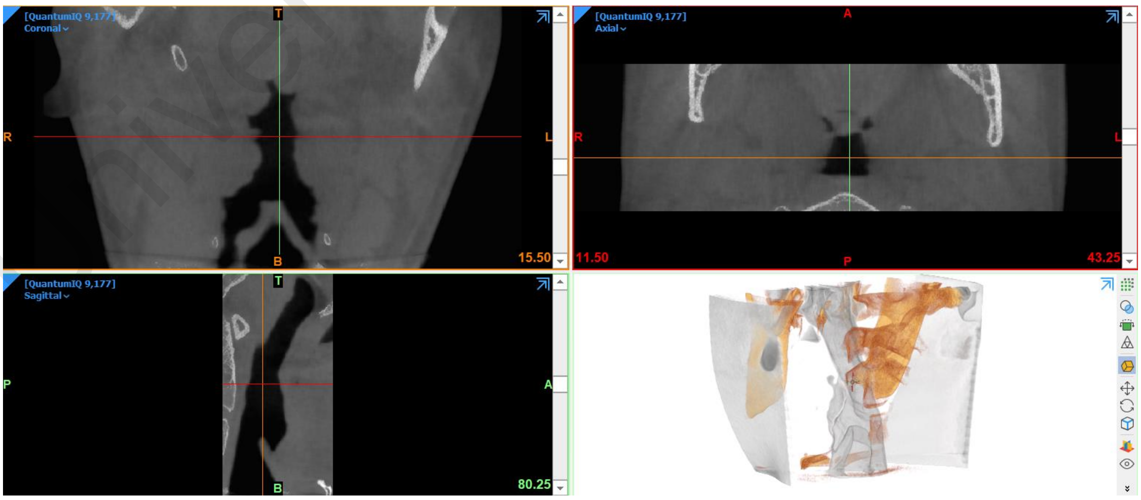

Figure 3.1: Pre-OP CT scan of the patient viewed using Mimics. Axial, coronal, sagittal and 3D views (counterclockwise starting from top right)

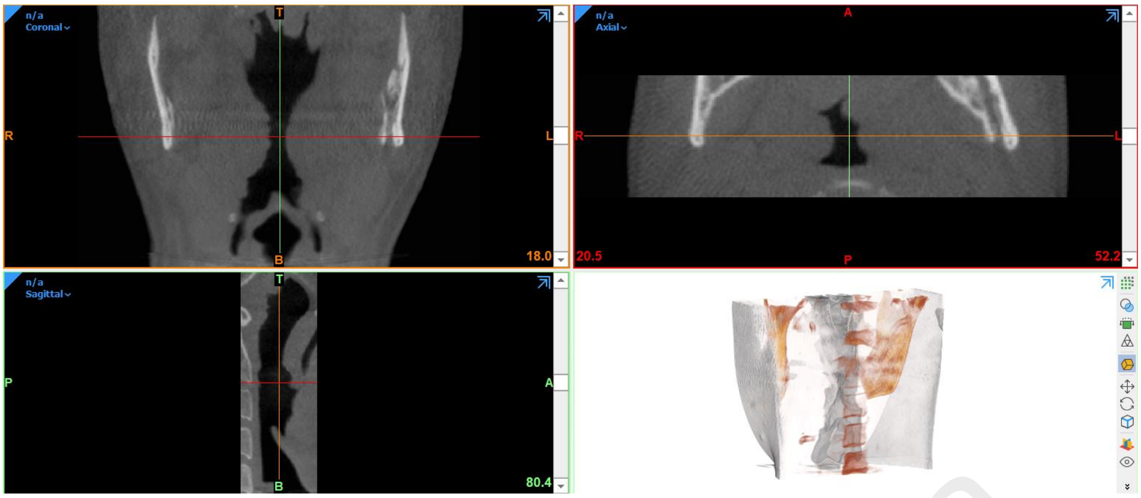

Figure 3.2: Post-OP CT scan of the patient viewed using Mimics. Axial, coronal, sagittal and 3D views (counterclockwise starting from top right)

The "Threshold" function in Mimics is utilized to segment the airway from pharyngeal wall. Based on the literature, the optimum threshold range for human respiratory airway is from -1024 to -500 HU. Hence, pixels within the following range are highlighted in green (known as "Mask") as shown in Figure 3.3 and 3.4. However, the region of interest is the velopharynx of the respiratory tract. Therefore, the area outside of the region is cropped from the mask and the "Region Grow" function is utilized to ensure all the pixels are selected. Subsequently, the 3D model is calculated and generated from the edited mask as shown in Figure 3.5 and 3.6.

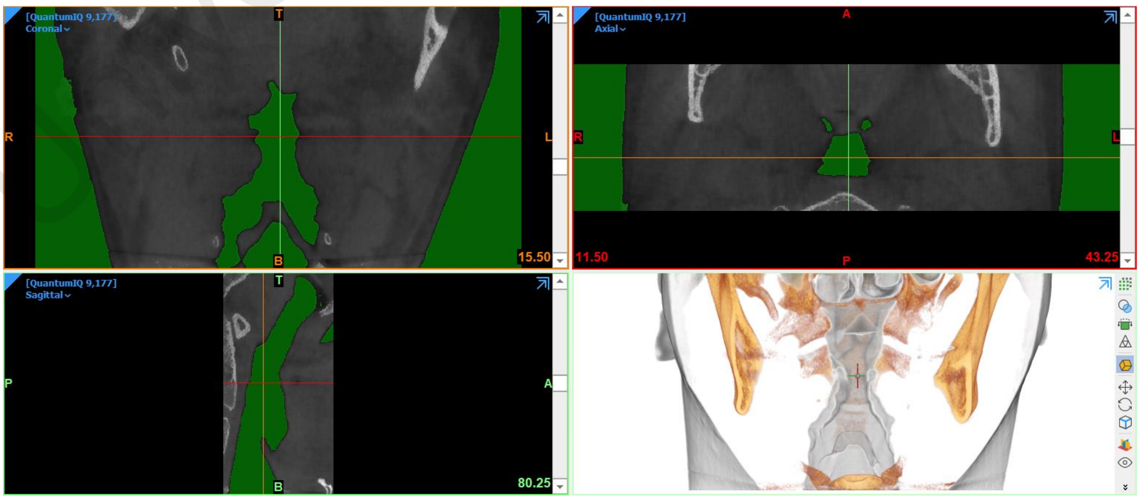

Figure 3.3: Thresholding of pre-OP CT scan to generate mask.

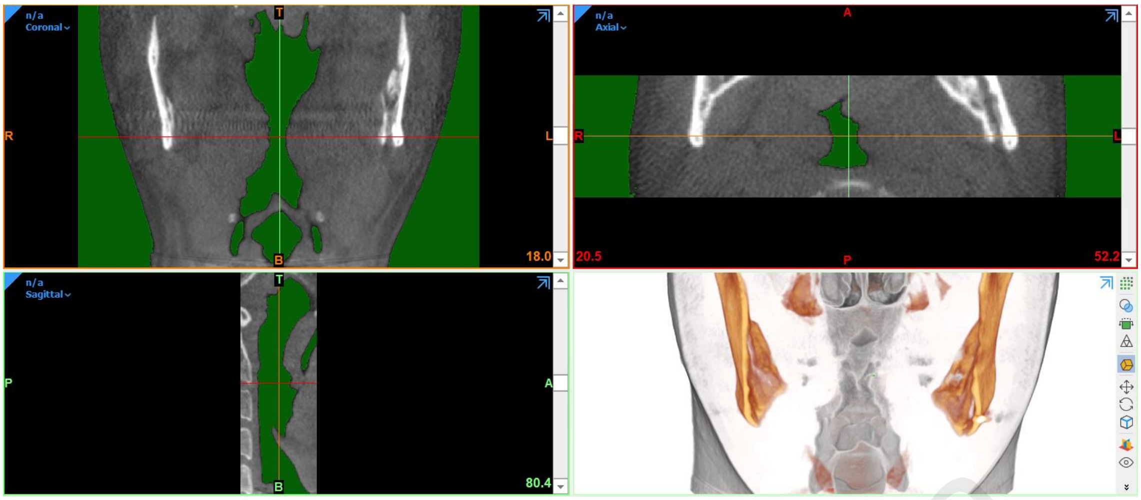

Figure 3.4: Thresholding of post-OP CT scan to generate mask.

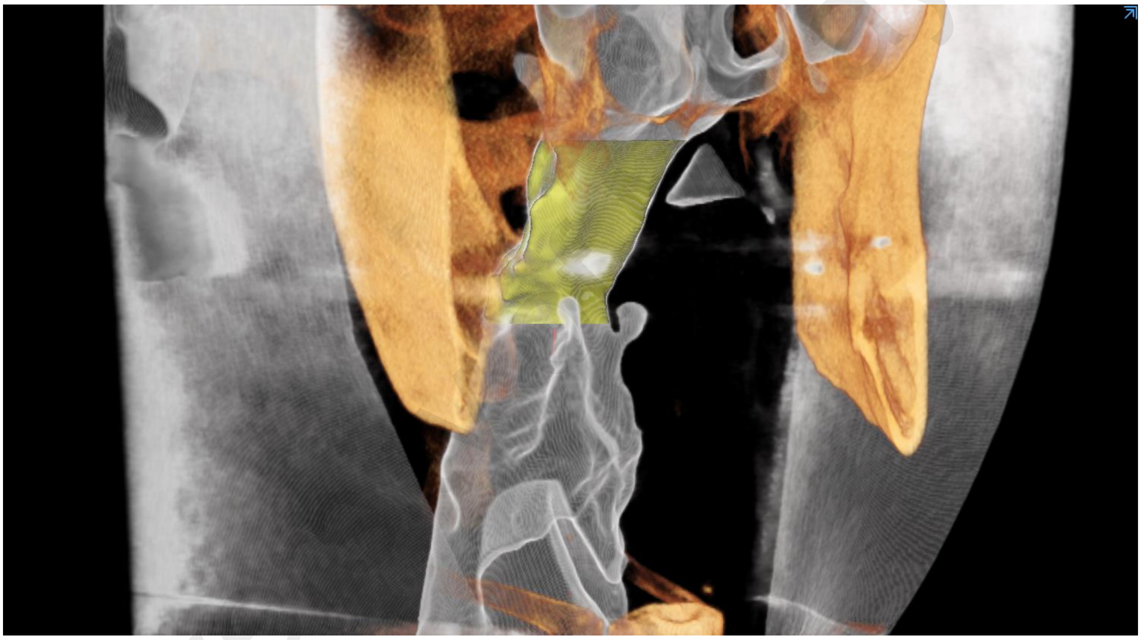

Figure 3.5: Pre-OP 3D model of the velopharynx region in the respiratory tract (yellow region).

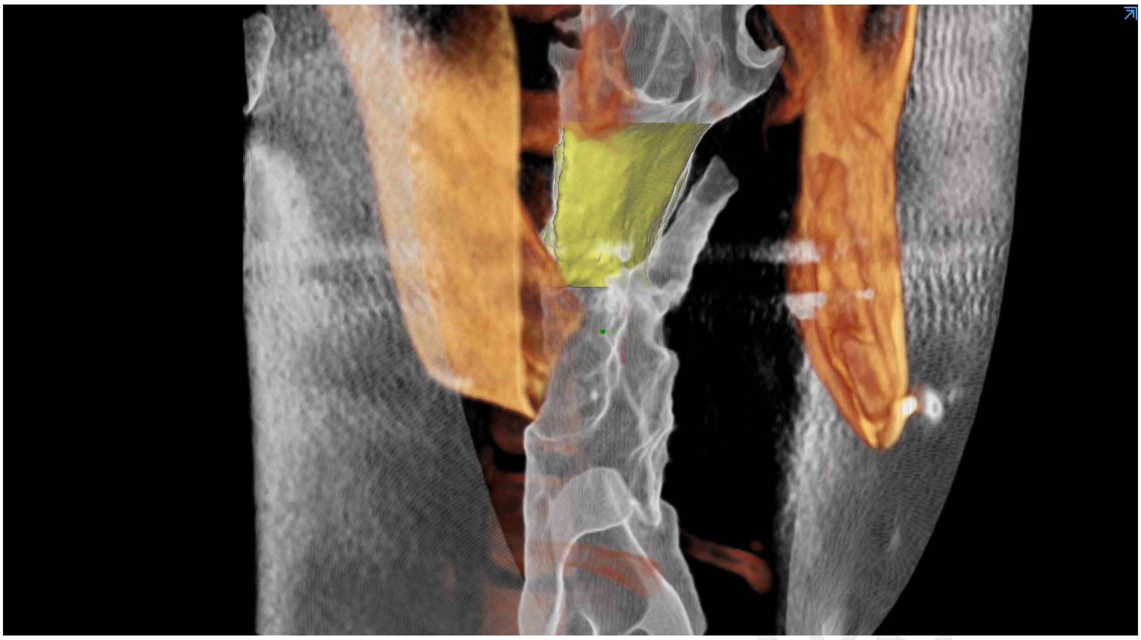

Figure 3.6: Post-OP 3D model of the velopharynx region in the respiratory tract (yellow region).

3.2 Mesh Generation

The mesh generation of the 3D models are performed using 3-Matic Research 13.0 (Materialise, Leuven, Belgium). The geometries generated in Mimics are imported into 3-Matic. The three major surfaces are named as wall, inlet, and outlet to streamline the simulation process. Inlet represents the surface nearest to the nasal cavity, while the outlet is the furthest surface and the wall is the wall of the velopharynx. Surface smoothing is applied to the wall prior to the mesh generation. This process removes uneven surfaces to reduce the number of skewed elements. In addition, the edge of the inlet and outlet is deselected during the smoothing process to maintain the geometry. Thereafter, the surface mesh and volume mesh are generated using “Adaptive Remesh” and “Create Volume Mesh” functions, respectively. The element length for the 2D surface triangles and 3D internal tetrahedrons are kept at maximum 0.5 mm, respectively. Hence, the number of volume elements generated for the pre-op model (Figure 3.7 and 3.8) and post-op model (Figure 3.9 and 3.10) are 1.04 million and 1.49 million, respectively.

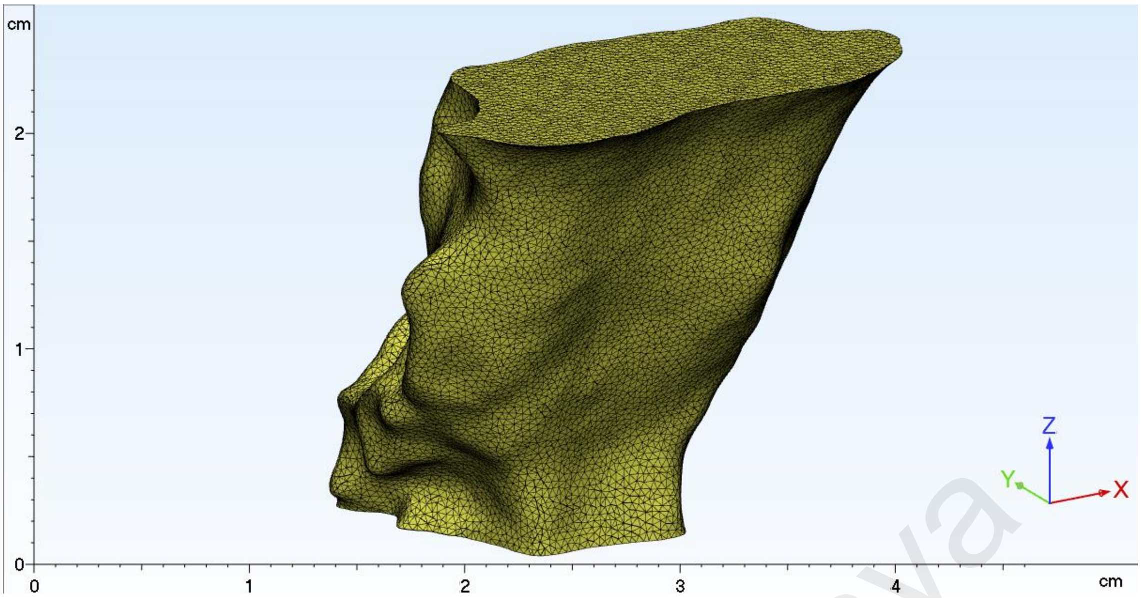

Figure 3.7: Surface elements of the pre-op model.

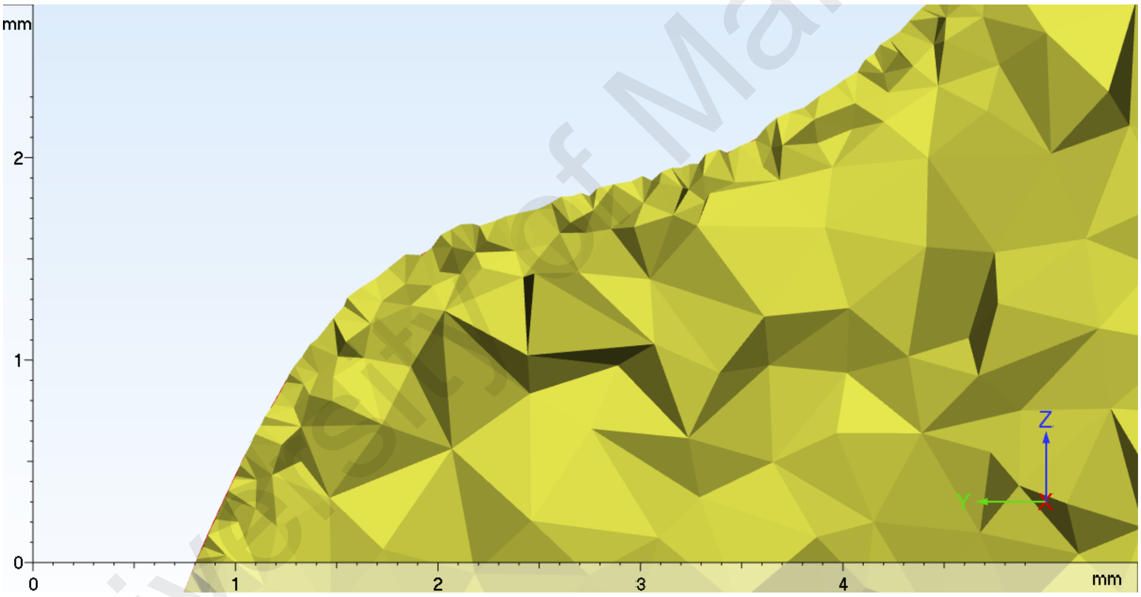

Figure 3.8: Enlarged view of the internal volume element of the pre-op model.

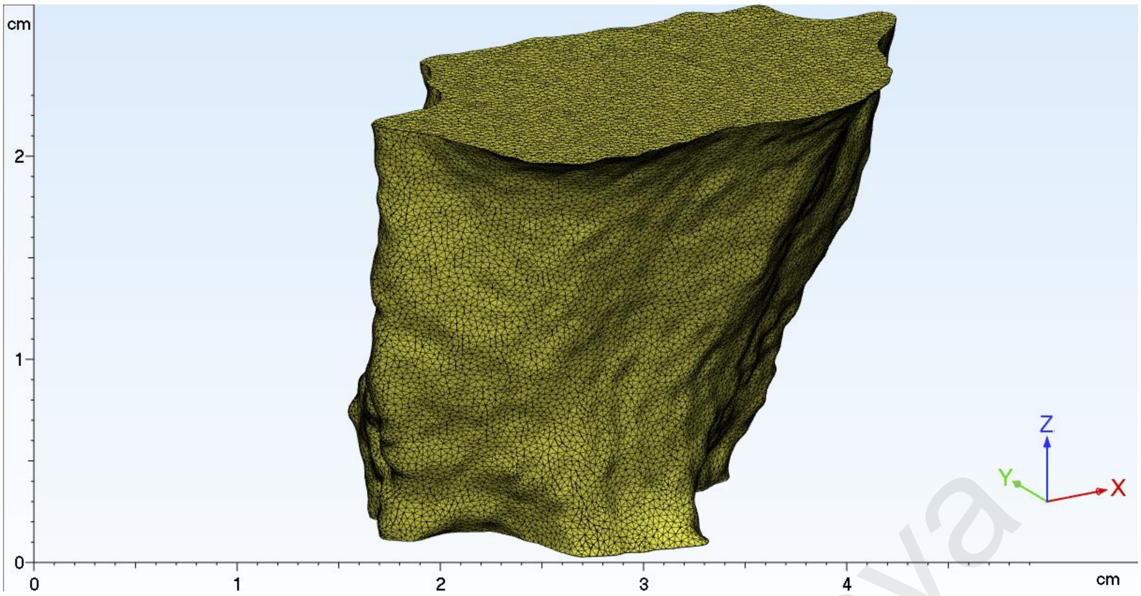

Figure 3.9: Surface elements of the post-op model.

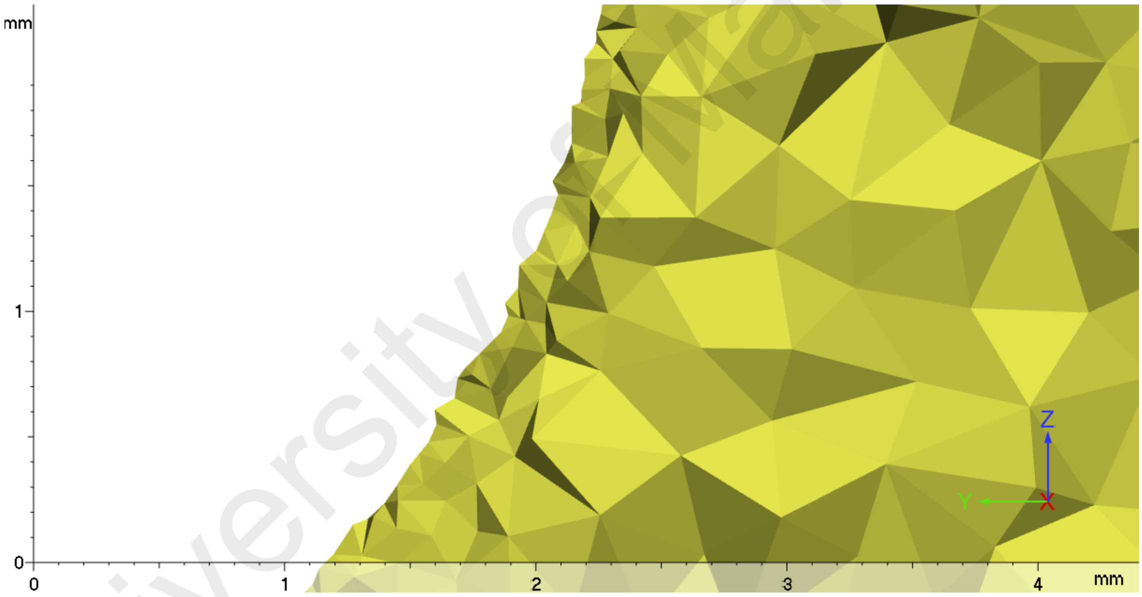

Figure 3.10: Enlarged view of the internal volume element of the post-op model.

3.3 Computational Fluid Dynamics Simulation

3.3.1 Governing Equations

As discussed in Chapter 2, the pharyngeal airflow is determined as steady and incompressible flow. In addition, flow studies below 0.2 L/s is assumed to be laminar and fully developed turbulent is achieved when flow exceeds 0.5 L/s. The continuity and momentum equations for steady and incompressible laminar flow are as follow:

$$\nabla \cdot \vec{u} = 0 \tag{3.1}$$

$$\frac{\partial \vec{u}}{\partial t} + \nabla \cdot (\vec{u}\vec{u}) + \frac{1}{\rho}\nabla p - v\nabla^2 \vec{u} = 0 \tag{3.2}$$

where $\vec{u}$ is the velocity vector, ρ is the density of fluid, p is the fluid pressure and v is the kinematic viscosity of fluid.

The fully developed turbulent flow is studied using k-ω model, therefore, two additional transport equations are required for turbulence kinetic energy and specific dissipation rate (Wilcox, 2008) are as follow:

$$\frac{\partial k}{\partial t} + \frac{\partial k u_j}{\partial x_j} = \tau_{ij}\frac{\partial u_j}{\partial x_j} - \beta^* \omega k + \frac{\partial}{\partial x_j}\left[\left(v + \sigma_k \frac{k}{\omega}\right)\frac{\partial k}{\partial x_j}\right] \tag{3.3}$$

$$\frac{\partial \omega}{\partial t} + \frac{\partial \omega u_j}{\partial x_j} = \alpha \frac{\omega}{k}\tau_{ij}\frac{\partial u_j}{\partial x_j} - \beta \omega^2 + \frac{\partial}{\partial x_j}\left[\left(v + \sigma_\omega \frac{k}{\omega}\right)\frac{\partial \omega}{\partial x_j}\right] \tag{3.4}$$

where k is the turbulence kinetic energy, ω is the specific dissipation rate, and τ_{ij} is the Reynolds stress tensor. Moreover, the constant parameters are given as: $\alpha = 0.555$, $\beta = 0.8333$, $\beta^* = 1$, and $\sigma_k = \sigma_\omega = 0.5$.

3.3.2 Numerical Methods

Numerical simulations are performed using Fluent 2020 R1 (Ansys, Canonsburg, Pennsylvania, United States). There are four pressure-based algorithms that uses pressure-velocity coupling schemes in Fluent, namely SIMPLE, SIMPLEC, PISO, and COUPLED. However, the PISO scheme has the least computational cost when compared to the other schemes in obtaining similar result (Kumar et al., 2019). Hence, the pressure and momentum terms are approached using PISO with second order upwind spatial discretization. In addition, the residuals are monitored using convergence criterion of 1×10^{-4}.

3.3.3 Mesh Independence Test

Mesh independence test is conducted by improving the volume element of the velopharynx model by using element length of 0.7 mm, 0.65 mm, 0.6 mm and 0.5 mm for both pre- and post-OP meshes. Hence, the number of volume elements generated for the pre- and post-OP geometry are listed in Table 3.1. However, convergence of the solution cannot be achieved using 0.6 mm element length, while the solution diverges for 0.7 mm and 0.65 mm meshes. Hence, the optimal number of elements are determined as 1,042,300 and 1,489,659 for pre- and post-OP, respectively.

Table 3.1: Number of 3D tetrahedral elements in each corresponding mesh.

Element length (mm)	Pre-OP	Post-OP
0.7	381,069	543,295
0.65	475,775	678,034
0.6	603,928	862,573
0.5	1,042,300	1,489,659

CHAPTER 4: RESULTS AND DISCUSSION

4.1 Morphology Effect of Maxillomandibular Advancement

The CT scans are taken before and after the MMA operation, therefore, physical changes can be observed through the geometry reconstruction. As the domain of interest is the velopharynx, the dimensions are measured and listed at Table 4.1. The volume of the region has enlarged by approximately 42%. In addition, the opening of the velopharynx has widen by approximately 71%.

Table 4.1: Comparison between pre- and post-op airway geometry.

	Pre-OP	Post-OP	Change
Inlet area (mm^2)	215.2034	366.9826	151.7792
Outlet area (mm^2)	143.0784	146.9447	3.8663
Velopharynx volume (mm^3)	3989.0196	5676.3654	1687.3458
Inlet perimeter (mm)	62.38	80.12	17.74

4.2 Computational Fluid Dynamics Turbulence Modeling

The turbulent airflow is simulated with constant volume flow rate of 0.5 L/s at the inlet of the model. However, the inlet velocity varies between the pre- and post-op due to the inlet area. Table 4.2 shows the properties obtained from the flow simulations. Lower pressure drop between the inlet and outlet is observed in the post-op airway.

In another pre- and post-MMA study, similar variation in pressure drop between two planes is observed as it has reduced from 53.8 Pa to 25.7 Pa (Kim et al., 2015). Although the pre- and post-op pressure drop is different, the percentage difference between pre- and post-op of both cases in similar.

Table 4.2: Airflow properties of turbulence modeling.

	Pre-OP	Post-OP	Difference
Inlet velocity (m/s)	2.2781	1.3273	0.9508
Max/min inlet pressure (Pa)	140.314/-2.0576	74.4933/3.5173	65.8307/5.5749
Max/min outlet pressure (Pa)	5.4224/-3.4093	2.6331/-3.5482	2.7893/0.13887
Mean inlet pressure (Pa)	71.1858	35.4880	35.6978
Mean outlet pressure (Pa)	4.4159	3.0907	1.3252
Pressure drop (Pa)	66.7699	32.3973	34.3726

The surface static pressure and velocity magnitude are shown at pre- and post-op in Figure 4.1 and 4.2. Aerodynamic activity occurs mainly at the anterior wall surface of the velopharynx. In addition, high pressure and low velocity in the inlet region while low pressure and high velocity in the outlet region as shown in Table 4.3. The pressure and velocity are obtained from the same location on the cross section. Moreover, the post-op airflow properties have decreased.

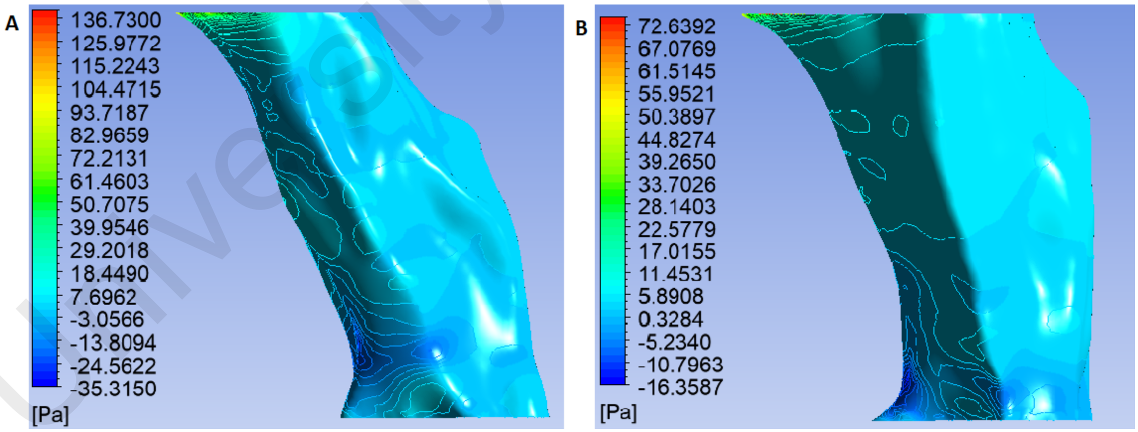

Figure 4.1: Wall surface pressure contour of (a) pre-op and (b) post-op velopharynx models.

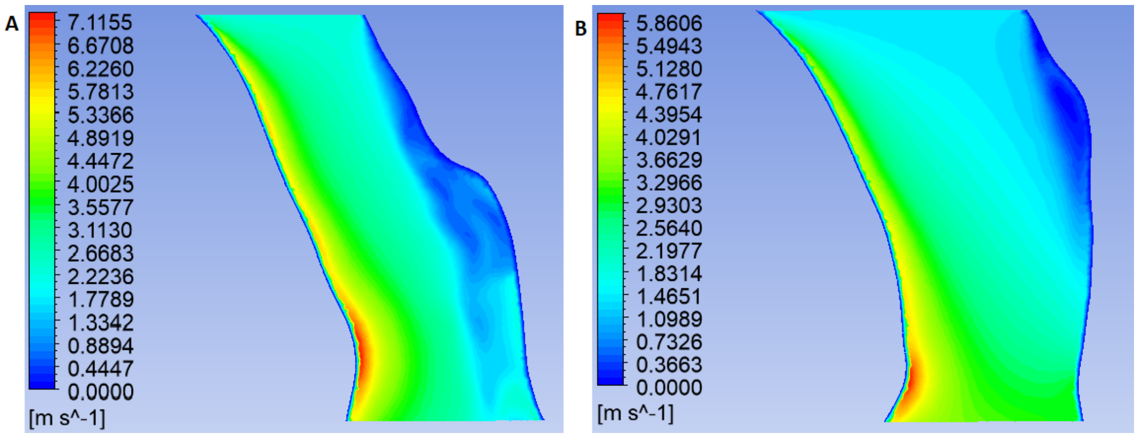

Figure 4.2: Velocity contour of (a) pre-op and (b) post-op velopharynx mid-sagittal plane.

Table 4.3: Airflow properties at the inlet and outlet region on the anterior wall of the velopharynx.

	Pre-OP	Post-OP	Difference
Inlet region pressure (Pa)	37.3239	22.1845	15.1394
Outlet region pressure (Pa)	-14.8400	-11.5026	3.3374
Inlet region velocity (m/s)	3.1415	1.7796	1.3619
Outlet region velocity (m/s)	7.1570	5.8990	1.2580

The turbulence kinetic energy and wall shear stress comparison are shown in Figure 4.3 and 4.4. Reduction of turbulence kinetic energy is observed at the anterior region of the velopharynx while it is no longer present in the posterior region. The high wall shear stress distribution shown in the Figure 4.4 further indicates aerodynamic activity on the anterior wall region.

The overall magnitude reduction of wall shear stress in the upper respiratory airway is observed in a comparison study of pre- and post-MMA operation (G. C. Cheng et al., 2014). Despite the narrow scope of study, similar observation is seen in the velopharynx region in both studies.

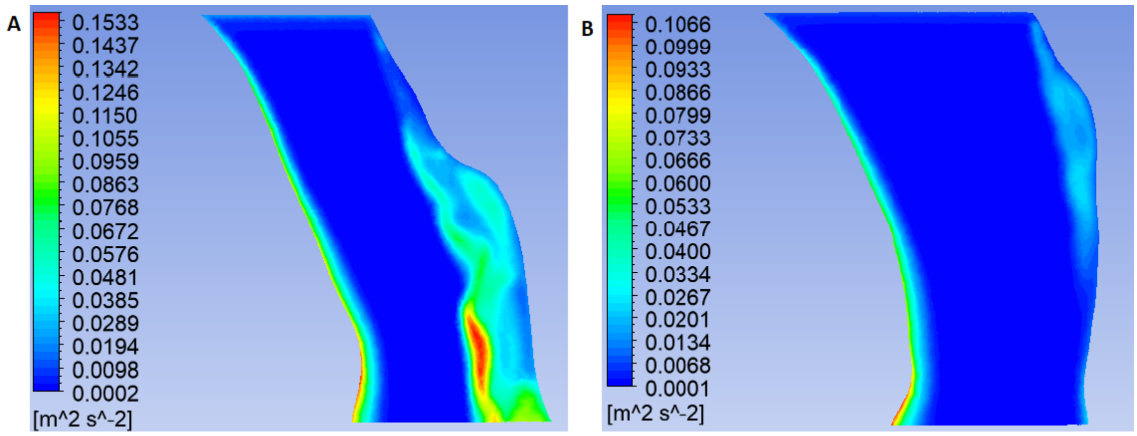

Figure 4.3: Turbulence kinetic energy contour of (a) pre-op and (b) post-op velopharynx mid-sagittal plane.

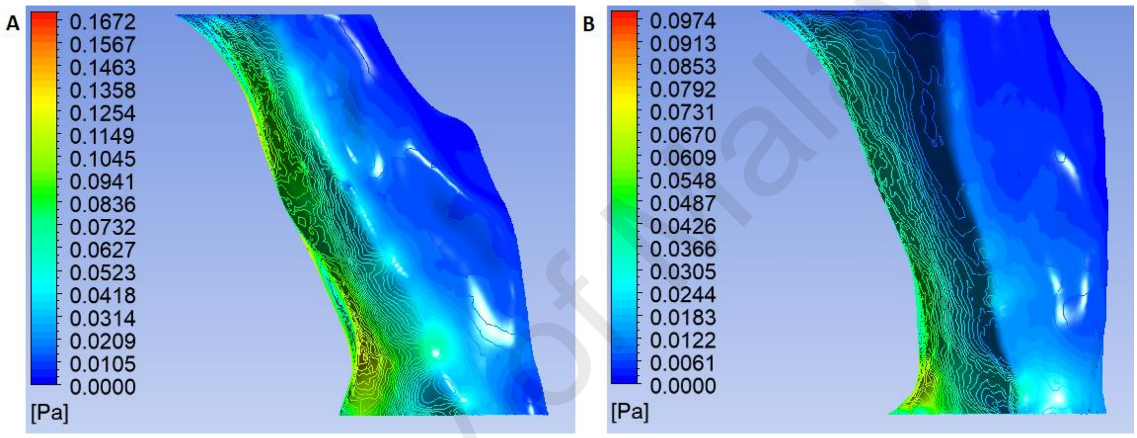

Figure 4.4: Wall shear stress contour of (a) pre-op and (b) post-op velopharynx models.

4.3 Turbulent Flow in the Domain

The Reynold number, Re is represented by the following equation:

$$\mathrm{Re} = \frac{\rho u D_h}{\mu} \tag{4.1}$$

where ρ is the density of fluid, u is the velocity of fluid, D_h is the equivalent hydraulic diameter, and μ is the dynamic viscosity of the fluid. The equivalent hydraulic diameter is obtain using the following equation:

$$D_h = \frac{4A}{P} \tag{4.2}$$

where A is the surface area and P is the surface perimeter.

The Reynolds number for pre- and post-op is 2152 and 1665, respectively. It is known that Re number below 2000 is classified as laminar flow and above 4000 is turbulent flow. However, the following range is explicitly for fluid flow in pipes. In addition, the irregularities in the human airway lowers the Re number of the turbulent flow (Kumar et al., 2019).

4.4 Collapsibility of the Soft Tissue

Literatures have stated OSA is due to the morphology the airway, mainly cause by the reduction of the cavity (Jeong et al., 2007; Sauerland & Harper, 1976; Schwab et al., 1993). In addition, the collapsibility of the soft tissue due to the dynamics and airflow in the airway is demonstrated in Figure 4.1(a). The negative pressure in comparison with the atmospheric would produce transverse pressure difference from the anterior wall to the posterior, resulting in the collapse of the upper airway. Moreover, the low-pressure region is located at the soft palate which does not contain bone structure to support the geometry.

4.5 Computational Fluid Dynamics Study on Maxillomandibular Advancement

CFD is vastly applied in simulating the respiratory tract, and studying the pressure, velocity, and turbulent kinetic energy of the airflow (Aasgrav et al., 2017; Azarnoosh et al., 2016; Srivastav et al., 2019; Wootton et al., 2016). In this study, the airflow of post-operation is compared to pre-operation to observe the characteristics of OSA in the respiratory tract. It is observed that the MMA surgery has increased the internal volume of the tract in the velopharynx region.

The results indicate an overall improvement in the aerodynamic properties of the airway. As observed in Table 4.2, the inlet pressure dropped from 71 Pa to 35 Pa, the outlet pressure dropped from 4 Pa to 3 Pa, and the pressure drop between the inlet and outlet has reduced by 51% after MMA. In addition, the inlet and outlet velocity on the anterior region decreased by 43% and 17%, respectively.

The results from this study corresponds with the conclusions by other researchers who analyzed the effect of maxillomandibular advancement on patients with obstructive sleep apnea by means of computational fluid dynamics (Ghoneima et al., 2015; Yu et al., 2009). They have stated that the cross-sectional area and volume of the respiratory tract increased after the operation. They have also indicated the reduction of the airflow properties.

CHAPTER 5: CONCLUSION AND RECOMMENDATIONS

5.1 Conclusion

The computed tomography of the patient with obstructive sleep apnea is successfully analyzed using the Materialised software, which includes Mimics Research and 3-Matic Research. The CT images are segmented to extract the airway of the respiratory tract. Thereafter, the geometry is generated and meshed. Ansys Fluent is used to simulate the turbulent flow of using k-ω scheme with second order upwind discretization. The effects of maxillomandibular advancement are analyzed by comparing the pre- and post-operation models. Based on the results, the overall parameters that causes OSA have improved after MMA. The pressure drop between inlet and outlet has reduced by 51% and the turbulent kinetic has decreased in the anterior region and no longer present in the posterior region.

5.2 Recommendations for Future Work

Due to the limitation of hardware, the scope of this study is narrowed down to reduce the computational cost of simulation. The LES and DNS approaches should be used to increase the definition of the result. Besides that, other solver schemes such as, SIMPLE, SIMPLEC, SIMPLER, and COUPLED should be used to cross-check the result. In addition, the whole pharyngeal airway should be modeled to increase the accuracy of the airflow simulation.

REFERENCES

Aasgrav, E., Johnsen, S. G., Simonsen, A. J., & Müller, B. (2017). *CFD simulations of turbulent flow in the human upper airways*. *2007*, 1–6. http://arxiv.org/abs/1706.02565

Azarnoosh, J., Sreenivas, K., & Arabshahi, A. (2016). CFD investigation of human tidal breathing through human airway geometry. *Procedia Computer Science*, *80*, 965–976. https://doi.org/10.1016/j.procs.2016.05.392

Bailie, N., Hanna, B., Watterson, J., & Gallagher, G. (2006). An overview of numerical modelling of nasal airflow. *Rhinology*, *44*(1), 53–57.

Bates, A. J., Schuh, A., Amine-Eddine, G., McConnell, K., Loew, W., Fleck, R. J., Woods, J. C., Dumoulin, C. L., & Amin, R. S. (2019). Assessing the relationship between movement and airflow in the upper airway using computational fluid dynamics with motion determined from magnetic resonance imaging. *Clinical Biomechanics*, *66*(October 2017), 88–96. https://doi.org/10.1016/j.clinbiomech.2017.10.011

Benchetrit, G. (2000). Breathing pattern in humans: Diversity and individuality. *Respiration Physiology*, *122*(2–3), 123–129. https://doi.org/10.1016/S0034-5687(00)00154-7

Cheng, G. C., Koomullil, R. P., Ito, Y., Shih, A. M., Sittitavornwong, S., & Waite, P. D. (2014). Assessment of surgical effects on patients with obstructive sleep apnea syndrome using computational fluid dynamics simulations. *Mathematics and Computers in Simulation*, *106*, 44–59. https://doi.org/10.1016/j.matcom.2012.11.008

Cheng, S., Gandevia, S. C., Green, M., Sinkus, R., & Bilston, L. E. (2011). Viscoelastic properties of the tongue and soft palate using MR elastography. *Journal of Biomechanics*, *44*(3), 450–454. https://doi.org/10.1016/j.jbiomech.2010.09.027

Cirignotta, F. (2004). Classification and definition of respiratory disorders during sleep. *Minerva Medica*, *95*(3), 177—185. http://europepmc.org/abstract/MED/15289747

Eckert, D. J., & Malhotra, A. (2008). Pathophysiology of adult obstructive sleep apnea. *Proceedings of the American Thoracic Society*, *5*(2), 144–153. https://doi.org/10.1513/pats.200707-114MG

Faizal, W. M., Ghazali, N. N. N., Badruddin, I. A., Zainon, M. Z., Yazid, A. A., Ali, M. A. bin, Khor, C. Y., Ibrahim, N. B., & Razi, R. M. (2019). A review of fluid-structure interaction simulation for patients with sleep related breathing disorders with obstructive sleep. *Computer Methods and Programs in Biomedicine*, *180*, 105036. https://doi.org/10.1016/j.cmpb.2019.105036

Faizal, W. M., Ghazali, N. N. N., Khor, C. Y., Badruddin, I. A., Zainon, M. Z., Yazid, A. A., Ibrahim, N. B., & Razi, R. M. (2020). Computational fluid dynamics modelling of human upper airway: A review. *Computer Methods and Programs in Biomedicine*, *196*, 105627. https://doi.org/10.1016/j.cmpb.2020.105627

Fan, Y., Dong, J., Tian, L., Inthavong, K., & Tu, J. (2020). Numerical and experimental analysis of inhalation airflow dynamics in a human pharyngeal airway. *International Journal of Environmental Research and Public Health*, *17*(5). https://doi.org/10.3390/ijerph17051556

Ghoneima, A., AlBarakati, S., Jiang, F., Kula, K., & Wasfy, T. (2015). Computational fluid dynamics analysis of the upper airway after rapid maxillary expansion: a case report. *Progress in Orthodontics*, *16*(1), 10. https://doi.org/10.1186/s40510-015-0085-x

Giles, TL, Lasserson, T., Smith, B., White, J., Wright, J., & Cates, C. (2006). Continuous positive airways pressure for obstructive sleep apnoea in adults. In Tammie Giles (Ed.), *Cochrane Database of Systematic Reviews*. John Wiley & Sons, Ltd. https://doi.org/10.1002/14651858.CD001106.pub3

Guilleminault, C., & Stoohs, R. (1990). Obstructive sleep apnea syndrome: whom to treat and how to treat. *Progress in Clinical and Biological Research*, *345*, 417–425.

Hagen, C., Gurumurthy, P., & Buzug, T. M. (2017). Effects of replacing the nasal cavity with a simple pipe like structure in CFD simulations of the airflow within the upper airways of OSA patients with patient individual flow rates. *Current Directions in Biomedical Engineering*, *3*(2), 795–798. https://doi.org/10.1515/cdbme-2017-0168

Hahn, I., Scherer, P. W., & Mozell, M. M. (1993). Velocity profiles measured for airflow through a large-scale model of the human nasal cavity. *Journal of Applied Physiology*, *75*(5), 2273–2287. https://doi.org/10.1152/jappl.1993.75.5.2273

Hochban, W., Brandenburg, U., & Peter, J. H. (1994). Surgical treatment of obstructive sleep apnea by maxillomandibular advancement. *Sleep*, *17*(7), 624–629. https://doi.org/10.1093/sleep/17.7.624

Hoffstein, V., & Szalai, J. P. (1993). Predictive value of clinical features in diagnosing obstructive sleep apnea. *Sleep*, *16*(2), 118–122. https://doi.org/10.1093/sleep/16.2.118

Hollandt, J. H., & Mahlerwein, M. (2003). Nasal Breathing and Continuous Positive Airway Pressure (CPAP) in Patients with Obstructive Sleep Apnea (OSA). *Sleep and Breathing*, *7*(2), 87–93. https://doi.org/10.1007/s11325-003-0087-7

Huang, Y., Malhotra, A., & White, D. P. (2005). Computational simulation of human upper airway collapse using a pressure-/state-dependent model of genioglossal muscle contraction under laminar flow conditions. *Journal of Applied Physiology*, *99*(3), 1138–1148. https://doi.org/10.1152/japplphysiol.00668.2004

Jeong, S. J., Kim, W. S., & Sung, S. J. (2007). Numerical investigation on the flow characteristics and aerodynamic force of the upper airway of patient with obstructive sleep apnea using computational fluid dynamics. *Medical Engineering and Physics*, *29*(6), 637–651. https://doi.org/10.1016/j.medengphy.2006.08.017

Johns, M. W. (1993). Daytime sleepiness, snoring, and obstructive sleep apnea; The Epworth Sleepiness Scale. *Chest*, *103*(1), 30–36. https://doi.org/10.1378/chest.103.1.30

Joosten, S. A., O'Driscoll, D. M., Berger, P. J., & Hamilton, G. S. (2014). Supine position related obstructive sleep apnea in adults: Pathogenesis and treatment. *Sleep Medicine Reviews*, *18*(1), 7–17. https://doi.org/10.1016/j.smrv.2013.01.005

Keyhani, K., Scherer, P. W., & Mozell, M. M. (1995). Numerical Simulation of Airflow in the Human Nasal Cavity. *Journal of Biomechanical Engineering*, *117*(4), 429–441. https://doi.org/10.1115/1.2794204

Kezirian, E. J., Goding, G. S., Malhotra, A., O'Donoghue, F. J., Zammit, G., Wheatley, J. R., Catcheside, P. G., Smith, P. L., Schwartz, A. R., Walsh, J. H., Maddison, K. J., Claman, D. M., Huntley, T., Park, S. Y., Campbell, M. C., Palme, C. E., Iber, C., Eastwood, P. R., Hillman, D. R., & Barnes, M. (2014). Hypoglossal nerve stimulation improves obstructive sleep apnea: 12-month outcomes. *Journal of Sleep Research*, *23*(1), 77–83. https://doi.org/10.1111/jsr.12079

Khalyfa, A., Gileles-Hillel, A., & Gozal, D. (2016). The Challenges of Precision Medicine in Obstructive Sleep Apnea. *Sleep Medicine Clinics*, *11*(2), 213–226. https://doi.org/10.1016/j.jsmc.2016.01.003

Kim, H. H., Rakibuzzaman, M., Suh, S. H., Kim, H. J., Choi, J. Y., & Lee, U. L. (2018). A study of fluid dynamics parameters for prediction of obstructive sleep apnea. *Journal of Mechanical Science and Technology*, *32*(3), 1079–1085. https://doi.org/10.1007/s12206-018-0210-0

Kim, H. H., Suh, S. H., Choi, J. Y., & Kim, T. (2015). Flow analyses of upper airway before and after maxillomandibular advancement surgery for obstructive sleep apnea patient. *Transactions of the Korean Society of Mechanical Engineers, B*, *39*(5), 443–448. https://doi.org/10.3795/KSME-B.2015.39.5.443

Kumar, B., Srivastav, V. K., Jain, A., & Paul, A. R. (2019). Study of numerical schemes for the CFD simulation of human airways. *International Journal of Integrated Engineering*, *11*(8), 32–40. https://doi.org/10.30880/ijie.2019.11.08.005

Lam, B., Sam, K., Mok, W. Y. W., Cheung, M. T., Fong, D. Y. T., Lam, J. C. M., Lam, D. C. L., Yam, L. Y. C., & Ip, M. S. M. (2007). Randomised study of three non-surgical treatments in mild to moderate obstructive sleep apnoea. *Thorax*, *62*(4), 354–359. https://doi.org/10.1136/thx.2006.063644

Lan, Z. (2004). Evaluation of pharyngeal volume and compliance of OSAHS patients using 3D CT and volume measurement. *Kanazawa Ika Daigaku Zasshi*, *29*(4), 243–251. http://inis.iaea.org/search/search.aspx?orig_q=RN:36081255

Launder, B. E., & Spalding, D. B. (1974). The numerical computation of turbulent flows. *Computer Methods in Applied Mechanics and Engineering*, *3*(2), 269–289. https://doi.org/10.1016/0045-7825(74)90029-2

Leong, S. C., Chen, X. B., Lee, H. P., & Wang, D. Y. (2010). A review of the implications of computational fluid dynamic studies on nasal airflow and physiology. *Rhinology*, *48*(2), 139–145. https://doi.org/10.4193/Rhin09.133

Lopez, S. J., Rahai, H., Taherian, S., & Hoang, H. (2019). *Applications of Computational Fluid Dynamics Simulation of the Upper Respiratory System*.

Mihaescu, M., Murugappan, S., Kalra, M., Khosla, S., & Gutmark, E. (2008). Large Eddy simulation and Reynolds-Averaged Navier-Stokes modeling of flow in a realistic pharyngeal airway model: An investigation of obstructive sleep apnea. *Journal of Biomechanics*, *41*(10), 2279–2288. https://doi.org/10.1016/j.jbiomech.2008.04.013

Mylavarapu, G., Mihaescu, M., Fuchs, L., Papatziamos, G., & Gutmark, E. (2013). Planning human upper airway surgery using computational fluid dynamics. *Journal of Biomechanics*, *46*(12), 1979–1986. https://doi.org/10.1016/j.jbiomech.2013.06.016

Nakano, H., Mishima, K., Ueda, Y., Matsushita, A., Suga, H., Miyawaki, Y., Mano, T., Mori, Y., & Ueyama, Y. (2013). A new method for determining the optimal CT threshold for extracting the upper airway. *Dentomaxillofacial Radiology*, *42*(3), 26397438. https://doi.org/10.1259/dmfr/26397438

Nakata, S., Noda, A., Yagi, H., Yanagi, E., Mimura, T., Okada, T., Misawa, H., & Nakashima, T. (2005). Nasal resistance for determinant factor of nasal surgery in CPAP failure patients with obstructive sleep apnea syndrome. *Rhinology*, *43*(4), 296–299.

Niinimaa, V., Cole, P., Mintz, S., & Shephard, R. J. (1980). The switching point from nasal to oronasal breathing. *Respiration Physiology*, *42*(1), 61–71. https://doi.org/10.1016/0034-5687(80)90104-8

Oksenberg, A., Silverberg, D., Offenbach, D., & Arons, E. (2006). Positional therapy for obstructive sleep apnea patients: A 6-month follow-up study. *Laryngoscope*, *116*(11), 1995–2000. https://doi.org/10.1097/01.mlg.0000237674.66716.a7

Ottaviano, G., Scadding, G. K., Coles, S., & Lund, V. J. (2006). Peak nasal inspiratory flow; normal range in adult population. *Rhinology*, *44*(1), 32–35.

Partinen, M. (1995). Epidemiology of obstructive sleep apnea syndrome. *Current Opinion in Pulmonary Medicine*, *1*(6), 482–487. https://doi.org/10.1097/00063198-199511000-00009

Pinto, J. A., de Mello Godoy, L. B., Marquis, V. W. P. B., Sonego, T. B., de Farias Aires Leal, C., & Ártico, M. S. (2011). Anthropometric data as predictors of obstructive sleep apnea severity. *Brazilian Journal of Otorhinolaryngology*, *77*(4), 516–521. https://doi.org/10.1590/S1808-86942011000400017

Quadrio, M., Pipolo, C., Corti, S., Messina, F., Pesci, C., Saibene, A. M., Zampini, S., & Felisati, G. (2016). Effects of CT resolution and radiodensity threshold on the CFD evaluation of nasal airflow. *Medical and Biological Engineering and Computing*, *54*(2–3), 411–419. https://doi.org/10.1007/s11517-015-1325-4

Roy, M., Becquemin, M. H., Bertholon, J. F., & Bouchikhi, A. (1994). Annexe B. Respiratory physiology. In *Annals of the ICRP* (Vol. 24, Issues 1–3, pp. 167–201). https://doi.org/10.1016/0146-6453(94)90040-X

Sauerland, E. K., & Harper, R. M. (1976). The human tongue during sleep: Electromyographic activity of the genioglossus muscle. *Experimental Neurology*, *51*(1), 160–170. https://doi.org/10.1016/0014-4886(76)90061-3

Schmidt-Nowara, W., Lowe, A., Wiegand, L., Cartwright, R., Perez-Guerra, F., & Menn, S. (1995). Oral appliances for the treatment of snoring and obstructive sleep apnea: A review. *Sleep, 18*(6), 501–510. https://doi.org/10.1093/sleep/18.6.501

Schreck, S., Sullivan, K. J., Ho, C. M., & Chang, H. K. (1993). Correlations between flow resistance and geometry in a model of the human nose. *Journal of Applied Physiology*, *75*(4), 1767–1775. https://doi.org/10.1152/jappl.1993.75.4.1767

Schwab, R. J., Gefter, W. B., Pack, A. I., & Hoffman, E. A. (1993). Dynamic imaging of the upper airway during respiration in normal subjects. *Journal of Applied Physiology*, *74*(4), 1504–1514. https://doi.org/10.1152/jappl.1993.74.4.1504

Schwab, R. J., Gupta, K. B., Gefter, W. B., Metzger, L. J., Hoffman, E. A., & Pack, A. I. (1995). Upper airway and soft tissue anatomy in normal subjects and patients with sleep-disordered breathing. Significance of the lateral pharyngeal walls. *American Journal of Respiratory and Critical Care Medicine*, *152*(5), 1673–1689. https://doi.org/10.1164/ajrccm.152.5.7582313

Sher, A. E. (2002). Upper airway surgery for obstructive sleep apnea. *Sleep Medicine Reviews*, *6*(3), 195–212. https://doi.org/10.1053/smrv.2002.0242

Srivastav, V. K., Paul, A. R., & Jain, A. (2019). Capturing the wall turbulence in CFD simulation of human respiratory tract. *Mathematics and Computers in Simulation*, *160*, 23–38. https://doi.org/10.1016/j.matcom.2018.11.019

Strobel, R. J., & Rosen, R. C. (1996). Obesity and weight loss in obstructive sleep apnea: A critical review. *Sleep*, *19*(2), 104–115. https://doi.org/10.1093/sleep/19.2.104

Sung, S.-J., Jeong, S.-J., Yu, Y.-S., Hwang, C.-J., & Pae, E.-K. (2006). Customized three-dimensional computational fluid dynamics simulation of the upper airway of obstructive sleep apnea. *The Angle Orthodontist*, *76*(5), 791–799. https://doi.org/10.1043/0003-3219(2006)076[0791:CTCFDS]2.0.CO;2

Tawhai, M. H., Hunter, P., Tschirren, J., Reinhardt, J., McLennan, G., & Hoffman, E. A. (2004). CT-based geometry analysis and finite element models of the human and ovine bronchial tree. *Journal of Applied Physiology*, *97*(6), 2310–2321. https://doi.org/10.1152/japplphysiol.00520.2004

Thatcher, G. W., & Maisel, R. H. (2003). The long-term evaluation of tracheostomy in the management of severe obstructive sleep apnea. *Laryngoscope*, *113*(2), 201–204. https://doi.org/10.1097/00005537-200302000-00001

Vos, W., de Backer, J., Devolder, A., Vanderveken, O., Verhulst, S., Salgado, R., Germonpre, P., Partoens, B., Wuyts, F., Parizel, P., & de Backer, W. (2007). Correlation between severity of sleep apnea and upper airway morphology based on advanced anatomical and functional imaging. *Journal of Biomechanics*, *40*(10), 2207–2213. https://doi.org/10.1016/j.jbiomech.2006.10.024

Wang, D. Y., Lee, H. P., & Gordon, B. R. (2012). Impacts of Fluid Dynamics Simulation in Study of Nasal Airflow Physiology and Pathophysiology in Realistic Human Three-Dimensional Nose Models. *Clinical and Experimental Otorhinolaryngology*, *5*(4), 181. https://doi.org/10.3342/ceo.2012.5.4.181

Wilcox, D. C. (2008). Formulation of the k-w Turbulence Model Revisited. *AIAA Journal*, *46*(11), 2823–2838. https://doi.org/10.2514/1.36541

Wilhelm, C. P., deShazo, R. D., Tamanna, S., Ullah, M. I., & Skipworth, L. B. (2015). The nose, upper airway, and obstructive sleep apnea. *Annals of Allergy, Asthma and Immunology*, *115*(2), 96–102. https://doi.org/10.1016/j.anai.2015.06.011

Williams, R. L., Karacan, I., & Moore, C. A. (1988). Sleep disorders: Diagnosis and treatment, 2nd ed. In R. L. Williams, I. Karacan, & C. A. Moore (Eds.), *Wiley series in general and clinical psychiatry.* John Wiley & Sons.

Wootton, D. M., Sin, S., Luo, H., Yazdani, A., McDonough, J. M., Wagshul, M. E., Isasi, C. R., & Arens, R. (2016). Computational fluid dynamics upper airway effective compliance, critical closing pressure, and obstructive sleep apnea severity in obese adolescent girls. *Journal of Applied Physiology*, *121*(4), 925–931. https://doi.org/10.1152/japplphysiol.00190.2016

Xu, C., Sin, S. H., McDonough, J. M., Udupa, J. K., Guez, A., Arens, R., & Wootton, D. M. (2006). Computational fluid dynamics modeling of the upper airway of children with obstructive sleep apnea syndrome in steady flow. *Journal of Biomechanics*, *39*(11), 2043–2054. https://doi.org/10.1016/j.jbiomech.2005.06.021

Yu, C.-C., Hsiao, H.-D., Lee, L.-C., Yao, C.-M., Chen, N.-H., Wang, C.-J., & Chen, Y.-R. (2009). Computational Fluid Dynamic Study on Obstructive Sleep Apnea Syndrome Treated With Maxillomandibular Advancement. *Journal of Craniofacial Surgery*, *20*(2), 426–430. https://doi.org/10.1097/SCS.0b013e31819b9671